One plasma sample was excluded from the pharmacokinetic analysis and was from the patient received constant subcutaneous infusion at steady state. Oxycodone concentration of this sample was 132 ng/mL, which indicated more than four-times higher than the geometric mean concentration (30.4 ng/mL) after constant subcutaneous infusion at steady state. This is considered because this patient took voriconazole, a strong CYP3A4 inhibitor, for treatment of complicated fungal infection for a few days before the blood sampling time.Co-administration of CYP3A4 inhibitor likely influenced the oxycodone pharmacokinetics in the patient. Oxycodone is metabolized by CYP3A4 to noroxycodone and by CYP2D6 to oxymorphone.[10, 16–18] Other patients did not take CYP3A4 inhibitors, CYP2D6 inhibitors[18], and CYP3A4 inducers[9] as concomitant medications before or during the blood sampling time. In this study, the influence of CYP3A4 inhibitors, CYP2D6 inhibitors, and CYP 3A4 inducers on oxycodone pharmacokinetics was not evaluated for noncompartmental analysis and population pharmacokinetic model analysis because no patients were co-administered with these inhibitors and inducers after exclusion of the plasma sample influenced by voriconazole.

The $t_{1/2,z}$ and CL of oxycodone after bolus intravenous administration which were estimated by noncompartmental analysis was 3.22 hours and 34,2 L/hour, respectively. The value of $t_{1/2,z}$ is similar but the value of CL is a little lower than those (48.6 and 45.4 L/hour) estimated in Australian patients with cancer pain after bolus intravenous administration reported by Leow et. al.[3], [6] The difference in CL is probably because there is difference in body size (Mean weight: 65.1 and 72.8 kg in Australian patients, 52.5 kg in Japanese patients) and there are limited sampling points (7 points) especially in the distribution phase in this study.

The geometric mean CLs estimated by the concentration at steady state were 24.3 and 29.5 L/hour after constant intravenous infusion and constant subcutaneous infusion, respectively. These values are similar to the geometric mean CL (30.4 L/hour) in Japanese patients with cancer pain by Kokubun et. al.[8] The geometric mean concentrations of noroxycodone and oxymorphone at steady state after constant intravenous infusion were 19.2 and 0.373 ng/mL and those after constant subcutaneous infusion were 14.4 and 0.386 ng/mL, respectively. The ratios of noroxycodone and oxymorphone to oxycodone concentrations were 0.520 and 0.01 after constant intravenous infusion, and 0.474 and 0.01 after constant subcutaneous infusion, respectively. These values are similar to the AUC ratios of noroxycodone (0.44) and oxymorphone (0.01) to oxycodone after intravenous administration in healthy volunteers by Nieminen et. al.[9] and AUC ratio of noroxycodone to oxycodone (0.45) after intramuscular administration in healthy volunteers by PÖYHIÄ et. al.[2] The limitation should be noted regarding the possibility of unreliable evaluation for concentrations at steady state in this study due to the limited PK blood samples and dose titration.

In population pharmacokinetic analysis, one-compartment model was selected using the plasma oxycodone concentration profile after constant infusion. One-compartment model were examined using the observed plasma oxycodone concentration profiles after bolus intravenous administration and constant intravenous and subcutaneous infusion at first. However, the plasma oxycodone concentration profile after bolus intravenous administration was described by bi-exponential phase and the pharmacokinetic parameters of the patients who received bolus intravenous administration were not estimated to describe overall concentration profiles adequately.

A two-compartment model was also examined but was not selected as a final model because model parameters were not estimated precisely for the patients who received constant infusion. This is probably due to the limited information in distribution phase. Infusion-type administration may be more popular and convenient than bolus administration in a clinical setting for patients with cancer pain. Therefore, we selected one-compartment model using the plasma oxycodone concentration data after constant infusion for population pharmacokinetic model.

Age, BWT, BSA, sex, and CLcr were found to be significant covariates on CL of oxycodone, and BSA was found to be the most important influencing factor on pharmacokinetics of oxycodone by population pharmacokinetic model building process. The result indicates that body size (BWT, BSA) is the most important factor on pharmacokinetics of oxycodone. Age and CLcr were not selected at the significant level of 1%. These factors were not selected as covariates of CL of controlled-release oxycodone by Charles.[19] However, Age and CLcr could be also important factors because pharmacokinetics of oxycodone is influenced by hepatic and renal function.[1] Komatsu et. al. reported that CL of oxycodone was influenced by Child-Pugh classification which was used to assess the prognosis of chronic liver disease.[20] Covariate related to hepatic function (AST, ALT) was not selected because there were little patients with hepatic impairment in our study. There were some reports that age did not influence the pharmacokinetic of oxycodone[19, 21–22] and other reports that CL of oxycodone was decreased in elderly people.[23–24] CL

of Oxycodone is influenced by some potential influence factors. Therefore contribution to influence CL by each single factor may be small. In our study, only BSA was selected in the final model because BWT, sex, and CLcr were highly or partly related to BSA as body size. Neither demographic nor clinical laboratory test data were selected as significant covariate on V of oxycodone. This is probably because there were insufficient data in the distribution phase and the information on V was limited. Final population pharmacokinetic model also indicates that lag time in absorption phase was 0.505 hours in subcutaneous infusion and there were no pharmacokinetic difference in CL and V between intravenous infusion and subcutaneous infusion.

There is the difference between the CL estimated from the data in bolus administration (34.2 L/hour) and the CL estimated from the population pharmacokinetic model (25.7 L/hour when BSA is 1.53). These CLs should not be affected by the mode of administration theoretically (bolus intravenous administration or intravenous infusion). Possible explanations for the difference in CL are that concentration data in the distribution phase and the elimination phase over 6 hours after bolus administration were limited and, therefore, the CL could not be adequately estimated by noncompartmental analysis.

The pharmacokinetics of oxycodone were evaluated extensively by noncompartmental analysis and population pharmacokinetic analysis using plasma concentration data from clinical studies in Japanese patients with cancer pain after intravenous or subcutaneous administration. These pharmacokinetic results provide the important information for the clinical use of oxycodone hydrochloride injection for the patients with cancer pain.

FUNDING

This study was funded by Shionogi & Co. Ltd., Osaka, Japan.

Declaration of interest: HK and MM received a consultancy fee from Shionogi & Co. Ltd. for their participation in this study. TY and MH declare no conflict of interest. HK, TY, MH and MM were not compensated for their work on this manuscript. KF is an employee of Shionogi & Co. Ltd.

REFERENCES

[1] Kalso E. Oxycodone. *J Pain Symptom Manage.* 2005;*29*:S47–56.

[2] Pöyhiä R, Seppälä T, Olkkola KT, Kalso E. The pharmacokinetics and metabolism of oxycodone after intramuscular and oral administration to healthy subjects. *Br J Clin Pharmacol.* 1992;*33*:617–21.

[3] Leow KP, Smith MT, Williams B, Cramond T. Single-dose and steady-state pharmacokinetics and pharmacodynamics of oxycodone in patients with cancer. *Clin Pharmacol Ther.* 1992b;*52*:487–95.

[4] Koizumi W, Toma H, Watanabe K, Katayama K, Kawahara M, Matsui K, et al. Efficacy and tolerability of cancer pain management with controlled-release oxycodone tablets in opioid-naive cancer pain patients, starting 5 mg tablets. *Jpn J Clin Oncol.* 2004;*34*:608–14.

[5] Narabayashi M, Saijo Y, Takenoshita S, Chida M, Shimoyama N, Miura T, et al. Opioid rotation from oral morphine to oral oxycodone in cancer patients with intolerable adverse effects: An open-label trial. *Jpn J Clin Oncol.* 2008;*38*:296–304.

[6] Leow KP, Cramond T, Smith MT. Pharmacokinetics and pharmacodynamics of oxycodone when given intravenously and rectally to adult patients with cancer pain. *Anesth. Analg.* 1995;*80*:296–302.

[7] Villesen HH, Banning AM, Petersen RH, Weinelt S, Poulsen JB, Hansen SH, et al. Pharmacokinetics of morphine and oxycodone following intravenous administration in elderly patients. *Therapeutics Clin Risk Manage.* 2007;*3*:961–7.

[8] Kokubun H, Fukawa M, Matoba M, Hoka S, Yamada Y, Yago K. Pharmacokinetics and variation in the clearance of oxycodone and hydrocotarnine in patients with cancer pain. *Biol Pharm Bull.* 2007;*30*:2173–7.

[9] Nieminen TH, Hagelberg NM, Saari TI, Pertovaara A, Neuvonen M, Laine K, et al. Rifampin greatly reduces the plasma concentrations of intravenous and oral oxycodone. *Anesthesiology.* 2009;*110*:1371–8.

[10] Saari TI, Grönlund J, Hagelberg NM, Neuvonen M, Laine K, Neuvonen PJ, et al. Effects of itraconazole on the pharmacokinetics and pharmacodynamics of intravenously and orally administered oxycodone. *Eur J Clin Pharmacol.* 2010;*66*:387–97.

[11] Beal SL, Sheiner LB, (eds.), NONMEM Users Guides, NONMEM Project Group, San Francisco, University of California at San Francisco, 1992.

[12] DuBois D, DuBois EF. A formula to estimate the approximate surface area if height and weight be known. *Arch Intern Med.* 1916;*17*:863–71.

[13] Cockcroft DW, Gault MH. Prediction of creatinine clearance from serum creatinine. *Nephron.* 1976;*16*:31-41

[14] Ette EI, Williams PJ, Kim YH, Lane JR, Liu MJ, Cappareli EV. Model appropriateness and population pharmacokinetics modeling. *J Clin Pharmacol.* 2003;*43*:610–23.

[15] Wings for NONMEM, Holford N.G. Available at http://wfn.sourceforge.net./ Accessed Jun 12, 2012

[16] Hagelberg NM, Nieminen TH, Saari TI, Neuvonen M, Neuvonen PJ, Laine K, et al. Voriconazole drastically increases exposure to oral oxycodone. *Eur J Clin Pharmacol.* 2009;*65*: 263–71.

[17] Nieminen TH, Hagelberg NM, Saari TI, Neuvonen M, Neuvonen PJ, Laine K, et al. Oxycodone concentrations are greatly increased by the concomitant use of ritonavir or lopinavir/ritonavir. *Eur J Clin Pharmacol.* 2010;*66*:977–85.

[18] Kummer O, Hammann F, Moser C, Schaller O, Drewe J, Krahenbuhl S. Effect of the inhibition of CYP3A4 or CYP2D6 on the pharmacokinetics and pharmacodynamics of oxycodone. *Eur J Clin Pharmacol.* 2011;*67*:63–71.

[19] Charles B, Hardy J, Anderson H, Tapuni A, George R, Norris R. Should the dosage of controlled-release oxycodone in advanced cancer be modified on the basis of patient characteristics? *Support Care Cancer.* 2014;*22*:325–30.

[20] Komatsu T, Kokubun H, Suzuki A, Takayanagi R, Yamada Y, Matoba M, et al. Population pharmacokinetics of oxycodone in patients with cancer-related pain. *J Pain Palliat Care Pharmacother*. 2012;*26*:220–5.

[21] Kaiko RF, Benziger DP, Fitzmartin RD, Burke BE, Reder RF, Goldenheim PD. Pharmacokinetic-pharmacodynamic relationships of controlled-release oxycodone. *Clin Pharmacol Ther*. 1996;*59*:52–61.

[22] Cherrier MM, Amory JK, Ersek M, Risler L, Shen DD. Comparative cognitive and subjective side effects of immediate-release oxycodone in healthy middle-aged and older adults. *J Pain*. 2009;*10*:1038–50.

[23] Saari TI, Ihmsen H, Neuvonen PJ, Olkkola KT, Schwilden H. Oxycodone clearance is markedly reduced with advancing age: a population pharmacokinetic study. *Br J Anaesth*. 2012;*108*:491–8.

[24] Liukas A, Kuusniemi K, Aantaa R, Virolainen P, Neuvonen M, Neuvonen PJ, et al. Plasma concentrations of oral oxycodone are greatly increased in the elderly. *Clin Pharmacol Ther*. 2008;*84*:462–7.

Received: 25 June 2014
Revised: 10 September 2014
Accepted: 12 September 2014

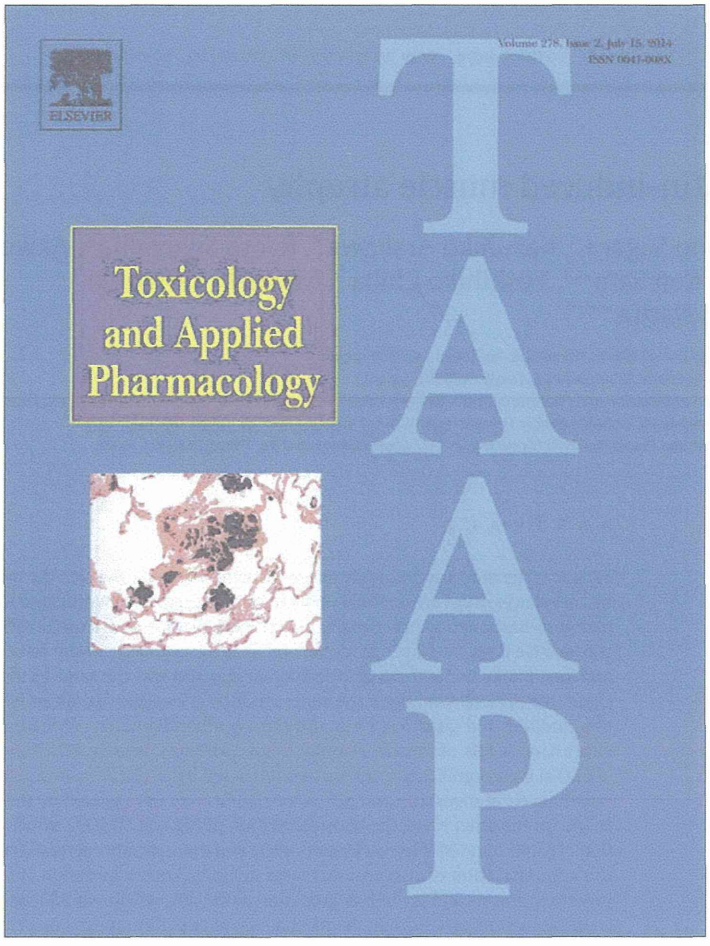

Toxicology and Applied Pharmacology 278 (2014) 190–199

Contents lists available at ScienceDirect

Toxicology and Applied Pharmacology

journal homepage: www.elsevier.com/locate/ytaap

Mechanisms of cisplatin-induced muscle atrophy

Hiroyasu Sakai [a,e,*], Atsunobu Sagara [a], Kazuhiko Arakawa [a], Ryoto Sugiyama [a], Akiko Hirosaki [a], Kazuhide Takase [a], Ara Jo [a], Ken Sato [a,e], Yoshihiko Chiba [b], Mitsuaki Yamazaki [c], Motohiro Matoba [d], Minoru Narita [a,**]

[a] Department of Pharmacology, Hoshi University, 2-4-41 Ebara, Shinagawa-ku, Tokyo 1428501, Japan
[b] Department of Biology, Hoshi University, 2-4-41 Ebara, Shinagawa-ku, Tokyo 1428501, Japan
[c] Department of Anesthesiology, Graduate School of Medicine and Pharmaceutical Sciences for Research, University of Toyama, 2630 Sugitani, Toyama-shi, Toyama 9300194, Japan
[d] Department of Palliative Medicine and Psychooncology, National Cancer Center Hospital, 5-1-1 Tsukiji, Chuo-ku, Tokyo 1040045, Japan
[e] Division of Pharmacy Professional Development and Research, Hoshi University, 2-4-41 Ebara, Shinagawa-ku, Tokyo 1428501, Japan

ARTICLE INFO

Article history:
Received 4 February 2014
Revised 23 April 2014
Accepted 1 May 2014
Available online 10 May 2014

Keyword:
Cisplatin
Muscle atrophy
Fatigue
Muscle atrophy F-box
Muscle RING finger-1

ABSTRACT

Fatigue is the most common side effect of chemotherapy. However, the mechanisms of "muscle fatigue" induced by anti-cancer drugs are not fully understood. We therefore investigated the muscle-atrophic effect of cisplatin, a platinum-based anti-cancer drug, in mice. C57BL/6J mice were treated with cisplatin (3 mg/kg, i.p.) or saline for 4 consecutive days. On Day 5, hindlimb and quadriceps muscles were isolated from mice. The loss of body weight and food intake under the administration of cisplatin was the same as those in a dietary restriction (DR) group. Under the present conditions, the administration of cisplatin significantly decreased not only the muscle mass of the hindlimb and quadriceps but also the myofiber diameter, compared to those in the DR group. The mRNA expression levels of muscle atrophy F-box (MAFbx), muscle RING finger-1 (MuRF1) and forkhead box O3 (FOXO3) were significantly and further increased by cisplatin treated group, compared to DR. Furthermore, the mRNA levels of myostatin and p21 were significantly upregulated by the administration of cisplatin, compared to DR. On the other hand, the phosphorylation of Akt and FOXO3a, which leads to the blockade of the upregulation of MuRF1 and MAFbx, was significantly and dramatically decreased by cisplatin. These findings suggest that the administration of cisplatin increases atrophic gene expression, and may lead to an imbalance between protein synthesis and protein degradation pathways, which would lead to muscle atrophy. This phenomenon could, at least in part, explain the mechanism of cisplatin-induced muscle fatigue.

Introduction

Chemotherapy compromises the patient's quality of life (QOL), an important indicator of patient outcome and survival in numerous cases (Montazeri, 2009). A component of QOL is the patient's perceived fatigue, which is one of the most common symptoms of cancer (Patrick et al., 2004). This type of fatigue is reported by cancer patients through QOL self-assessments and increases with the aggressiveness of chemotherapy (Cella et al., 2002; Prue et al., 2010; Stromgren et al., 2002; Wu and McSweeney, 2004). Over half of patients undergoing chemotherapy exhibit cognitive impairment (Jansen et al., 2011), which is associated with the patient's perceived fatigue (Bender et al., 2006). Although the documentation of perceived fatigue is useful clinically, it is difficult to discriminate this from physiological fatigue. Physiological fatigue can be divided into two components, central and peripheral. Central fatigue involves the central nervous system and the inhibition of neurological reflexes, whereas peripheral fatigue is more likely to be muscle-specific. Muscle fatigue is defined as a loss of force that can be reversed with rest, while muscle weakness is an impaired ability to generate force and is not relieved by rest (Wanner et al., 1990).

Muscle mass is maintained through an interplay between anabolic and catabolic pathways. The insulin-like growth factor-1 (IGF-1)/PI3K/Akt/ mammalian target of rapamycin (mTOR) pathway along with the ubiquitin–proteasome pathway and myostatin (Mstn) pathway maintain this homeostasis with the aid of various transcriptional and genetic factors (Banerjee and Guttridge, 2012). The activation of IGF-1 and Mstn signaling causes muscle hypertrophy and atrophy, respectively. Skeletal muscle atrophy is a debilitating consequence of multiple chronic diseases and conditions that involve starvation. It reduces treatment options and positive clinical outcomes as well as compromising QOL and increasing morbidity and mortality (Lynch, 2001; Zinna and Yarasheski, 2003). While considerable research has been undertaken to identify the molecular mechanisms that control skeletal muscle

* Correspondence to: H. Sakai, Department of Pharmacology, School of Pharmacy, Hoshi University, 2-4-41 Ebara, Shinagawa-ku, Tokyo 142-8501, Japan. Fax: +81 3 5498 5787.
** Correspondence to: M. Narita, Department of Pharmacology, School of Pharmacy, Hoshi University, 2-4-41 Ebara, Shinagawa-ku, Tokyo 142-8501, Japan. Fax: +81 3 5498 5784.
E-mail addresses: sakai@hoshi.ac.jp (H. Sakai), narita@hoshi.ac.jp (M. Narita).

http://dx.doi.org/10.1016/j.taap.2014.05.001
0041-008X/

atrophy, the signaling pathways involved and effective treatments that are currently available to prevent, attenuate or reverse muscle atrophy are not clearly defined.

ActRIIB is a high affinity activin type 2 receptor and mediates the signaling by a subset of TGF-β family ligands including Mstn, activin, and others (Lee, 2008). Increased signaling by the ActRIIB pathway has been implicated in many cancers (Costelli et al., 2008; Seder et al., 2009; Wildi et al., 2001). Zhou et al. (2010) has been demonstrated that in cancer cachexia models, ActRIIB pathway blockade abolished the activation of the ubiquitin–proteasome system and the induction of muscle-specific E3 ubiquitin ligases in muscles.

The discovery of two muscle-specific E3 ubiquitin ligases, Muscle atrophy F-Box (MAFbx; also known as atrogin-1) and Muscle RING Finger-1 (MuRF1), prompted renewed interest in identifying muscle-specific targets for therapeutic manipulation. MAFbx and MuRF1 are parts of the ubiquitin–proteasome pathway, which is the primary pathway involved in intracellular protein degradation in skeletal muscle (Lecker et al., 1999). Consistent increases in their gene expression have been observed in a wide range of in vivo models of skeletal muscle atrophy including diabetes, cancer, renal failure, denervation, unweighting and glucocorticoid or cytokine treatment (Bodine et al., 2001; Gomes et al., 2001). The expression of MAFbx and MuRF-1 mRNAs increases dramatically in catabolic states and mice deficient in either of them are partially resistant to muscle atrophy. Therefore, it is most likely that MAFbx and MuRF-1 play crucial roles in the loss of muscle proteins and their mRNAs are now considered to be specific markers of atrophy.

Chemotherapy generally consists of the administration of anti-cancer drugs in a standardized treatment regimen, which is specific for the type of cancer. Cisplatin, a platinum-based anti-cancer drug, is one of the most effective broad-spectrum anti-cancer drugs used against cervical, head and neck, prostrate, breast, lung, testicular and ovarian cancers. However, fatigue, including muscle fatigue, is the most common side effect of cisplatin after/during treatment. Damrauer et al. (2008) previously has been reported that the effect of cisplatin on muscle wasting was mediated through activation of the NF-κB signaling pathway. However, few reports have addressed the mechanisms that underlie cisplatin-induced muscle atrophy. In the present study, we investigated the mechanisms of cisplatin-induced muscle fatigue.

Methods

Animals. Male C57BL/6J mice (8–9 weeks of age, 23–27 g) were used. All experiments were approved by the Animal Care Committee at Hoshi University (Tokyo, Japan).

Treatment protocol. Mice were given a single intraperitoneal injection of cisplatin (1 or 3 mg/kg) daily for 4 days, with saline (vehicle) used as a control (Fig. 1A). As the body weight of mice was decreased by the administration of cisplatin, we prepared dietary restriction (DR) as another vehicle control by carrying out pair feeding. Only 2, 2, 2 and 1.5 g meal and 4, 4, 3 and 3 mL water were given to the DR mouse at Days 0–1, 1–2, 2–3 and 3–4. Twenty-four hours after the final injection of cisplatin (Day 3), animals were killed under deep anesthesia with isoflurane, and the femoral quadriceps and hind limb muscles were removed, and their wet weight were measured. In RT-quantitative PCR (qPCR), quadriceps muscle and liver were removed, washed with cold saline, and stored in TRI Reagent™ (Sigma-Aldrich) at −80 °C. Referred to previous reports (Fujimoto, 2006; Khasabova et al., 2012), we injected cisplatin (1, 3 and 10 mg/kg) to the mice daily for 4 days in our preliminary study. As the mouse injected with cisplatin (10 mg/kg), 3 mice in 5 mice died. We thus determined the given dose as 3 mg/kg, i.p.

Histology. Standard hematoxylin and eosin (HE) staining was performed on quadriceps muscle from cisplatin or its vehicle treated mice. Briefly, the quadriceps muscle was removed from anesthetized mice, and then fixates with 10% formalin for paraffin embedding and sectioning followed by HE staining. To analyze the length of the longest minor axis (the perpendicular bisector of the major axis) as diameters of the myofibers, the sections were observed under a light microscope in quadriceps muscles using the ImagePro Plus (Media Cybernetics, Silver Spring, MD) as shown Fig. 2A. For each animal at least 100 fibers were measured.

RT-qPCR. mRNA levels of cytokines and AQPs were examined by real-time RT-PCR as described previously (Sakai et al., 2013). Briefly, total RNA was extracted from various tissues with a one-step guanidium–phenol–chloroform extraction procedure using TRI Reagent™ (Sigma-Aldrich). cDNAs were prepared from total RNA (1.0 μg) by using QuantiTect Reverse Transcriptase (Qiagen, Germany) after incubation with gDNA wipeout buffer at 42 °C for 3 min to remove contaminating genomic DNA. The reaction mixture (2 μL) was subjected to PCR (50 nM forward and reverse primers, Fast SYBR Green Mastermix; Applied Biosystems) in a final volume of 10 μL. The PCR primer sets used are shown in Table 1. The thermal cycle profile used was 1) denaturing for 30 s at 95 °C, and 2) annealing for 30 s at 60 °C. PCR amplification was performed for 40 cycles. Data are expressed as the expression relative to GAPDH mRNA as a housekeeping gene using the $2^{-\mathrm{deltadeltaCT}}$ method (Sakai et al., 2013). In the case of tissue distribution of gene expression, data are expressed as the expression relative to 18 s rRNA as a housekeeping gene using the $2^{-\mathrm{deltadeltaCT}}$ method.

Immunoblotting. Homogenates of quadriceps muscle were prepared as follows. In brief, the muscle tissues were removed and immediately soaked in ice-cold, saline. The tissue was then homogenized in ice-cold T-PER™ Tissue Protein Extraction Reagent (Pierce). The tissue homogenate was centrifuged (1000 ×g, 4 °C for 15 min), and supernatants were stored at −80 °C until use. To quantify the phosphorylation of Akt and forkhead box 3a (FOXO3a), Western blotting was performed. In brief, the samples (10 μg of total protein per lane) were subjected to 10–20% sodium dodecyl sulfate-polyacrylamide gel electrophoresis (SDS-PAGE). The proteins were then electrophoretically transferred to a PVDF (polyvinylidene difluoride) membrane. After being blocked with 3% bovine serum albumin, transferred PVDF membranes were incubated with the primary antibodies. Rabbit anti-MuRF1 (1:1000 dilution; ECM Biosciences), rabbit anti-MAFbx (1:1000 dilution; ECM Biosciences), rabbit anti-FOXO3a (1:1000 dilution; Cell Signaling), rabbit anti-Akt (1:1000; Cell Signaling), rabbit anti-phospho-Akt (1:1000; Cell Signaling), rabbit anti-phospho-FOXO3a (1:1000; Cell Signaling), rabbit anti-Smad2 (1:1000; Cell Signaling) and rabbit anti-phosphor-Smad (1:1000; Cell Signaling) were used as a primary antibody. The membranes were then incubated with horseradish peroxidase-conjugated goat anti-rabbit immunoglobulin (Ig) G (1:5000 dilution; GE Healthcare), and detection was performed with an ECL system. The housekeeping gene was detected on the same membrane by using monoclonal mouse anti-GAPDH (1:5000 dilution; Chemicon International) and horseradish peroxidase-conjugated sheep anti-mouse IgG (1:5000 dilution; GE Healthcare) to confirm that the same amounts of proteins were loaded. To normalize the phosphorylated protein contents to the total protein, the ratio of the corresponding phosphorylated Akt or FOXO3a to total Akt or FOXO3a were calculated as an index of phospho-Akt or phospho-FOXO3a. In the level of protein expression, to normalize the Akt or FOXO3a contents to GAPDH, the ratio of the corresponding Akt or FOXO3a to GAPDH was calculated as an index of Akt or FOXO3a.

Statistical analysis. The statistical significance of differences was determined by an unpaired Student t-test or one-way analysis of

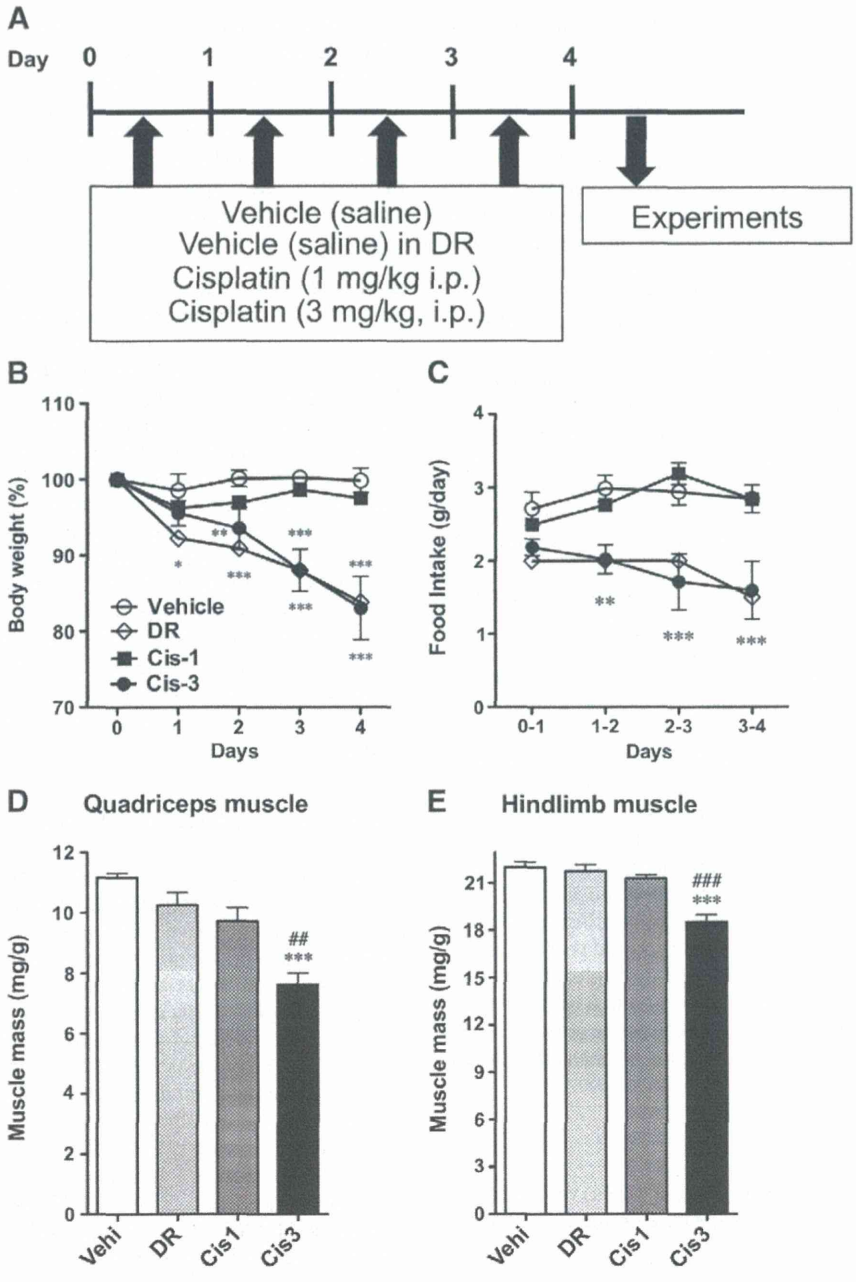

Fig. 1. Effect of cisplatin on the body weight, food intake and hindlimb and quadriceps muscle mass in the mouse. Schedule for the administration of vehicle (saline), vehicle + dietary restriction (DR, Days 0–1; 2 g, Days 1–2; 2 g, Days 2–3; 2 g and Days 3–4; 1.5 g) or cisplatin (3 mg/kg, i.p.) (A). Cisplatin or vehicle (saline, i.p.) was administered on Days 0–3. Twenty-four hours after the final administration of cisplatin or vehicle, experiments were performed. Effects of cisplatin (Cis-1; cisplatin 1 mg/kg, Cis-3; cisplatin 3 mg/kg) and DR on body weight and food intake (B and C). Effects of DR and cisplatin cisplatin (Cis-1; cisplatin 1 mg/kg, Cis-3; cisplatin 3 mg/kg) on hindlimb (D) and quadriceps (E) muscle mass. Each point or value represents the mean ± S.E.M. from 3 to 8 independent mice. *$p < 0.05$, **$p < 0.01$ and ***$p < 0.001$ vs. vehicle control (saline). ##$p < 0.01$ and ###$p < 0.001$ vs. DR.

variance (ANOVA) with the Bonferroni/Dunn post hoc-test. A value of $p < 0.05$ was considered significant.

Results

Effect of cisplatin on the body weight and food intake

The body weight of mice was significantly decreased by the administration of cisplatin (3 mg/kg, i.p.), but not 1 mg/kg, and dietary restriction (DR) to the same degree (Fig. 1B). Food intake was also significantly decreased by the administration of cisplatin (3 mg/kg, i.p.) and DR groups, and the similar changes are observed in those groups (Fig. 1C).

Cisplatin-induced muscle atrophy

Under these conditions, the administration of cisplatin (3 mg/kg, i.p.) significantly decreased the hindlimb and quadriceps muscle mass compared to those in the vehicle and DR groups (Figs. 1D and E). We next performed a morphometric analysis of the quadriceps muscle in the vehicle, DR and cisplatin (3 mg/kg, i.p.) groups. The myofiber diameters were significantly decreased by the administration of cisplatin compared to those in the vehicle and DR groups (Figs. 2B–E).

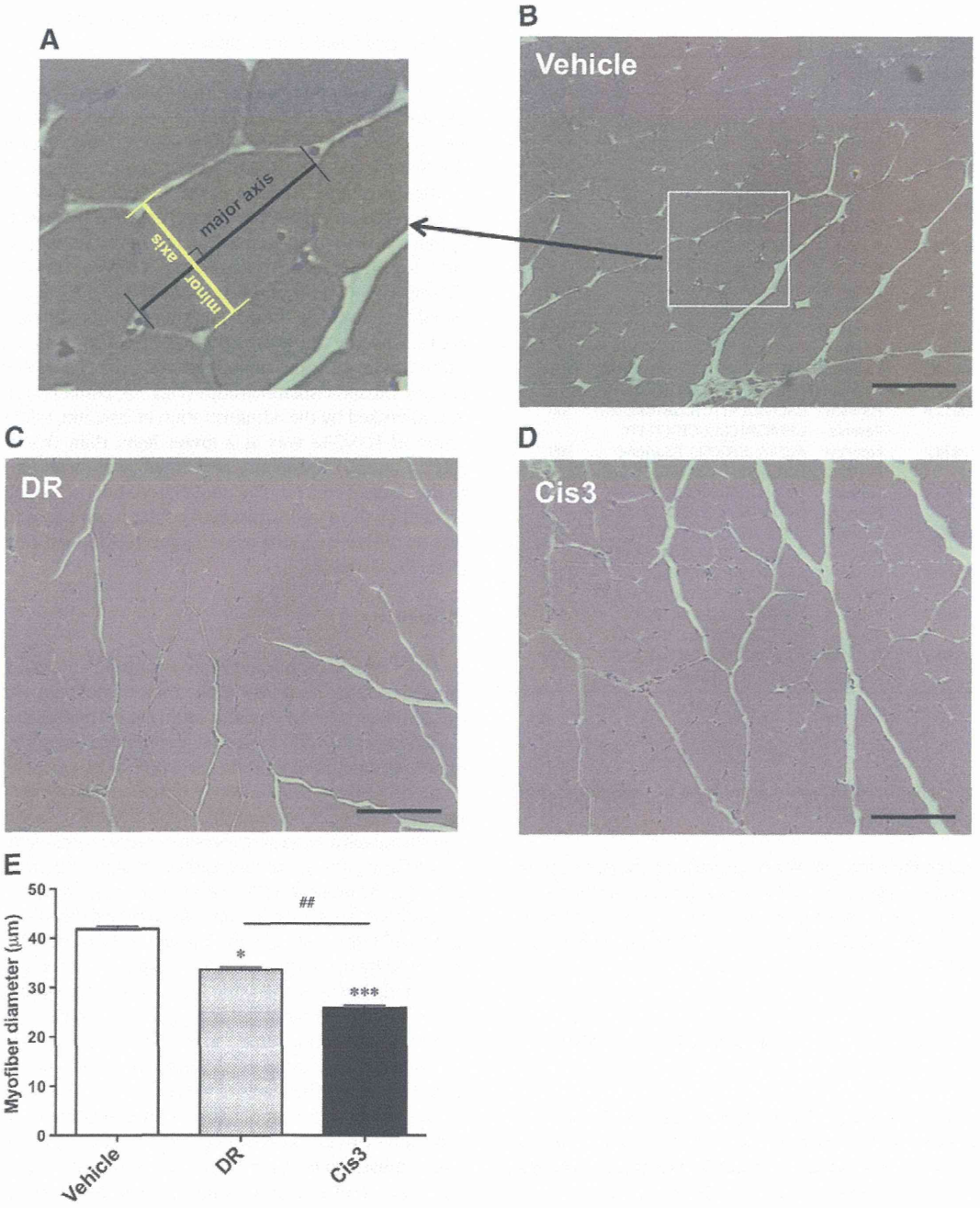

Fig. 2. Cisplatin-induced muscle atrophy. Hematoxylin–eosin staining of quadriceps muscle in the vehicle control (B), DR (C) and cisplatin groups (D). Typical the length of myofiber diameter (minor axis) is shown in (A). Bar scale: 100 μm. Effects of DR or cisplatin (3 mg/kg, i.p.; Cis) on myofiber diameter (D). Each point or value represents the mean ± S.E.M. from 3 to 4 independent mice. *$p < 0.05$ and ***$p < 0.001$ vs. vehicle control (saline). ##$p < 0.01$ and ###$p < 0.001$ vs. DR.

Effects of DR and cisplatin on the gene expression of MAFbx and MuRF1 in the muscle

Fasting-induced muscle wasting/atrophy is associated with increased levels of the E3 ubiquitin ligases MAFbx and MuRF1 (Bodine et al., 2001; Gomes et al., 2001). The expression levels of MAFbx and MuRF1 were significantly increased in the DR group compared to the vehicle control, and these levels were further increased by the administration of cisplatin (Figs. 3A and B). Casitas B-cell lymphoma proto-oncogene b (Cbl-b) and lysine 63-linked autoubiquitination of TNF receptor associated factor 6 (TRAF6) are also classified as E3 ubiquitin ligases (Nakao et al., 2009; Paul et al., 2012). In the present study, there was no difference in mRNA expression levels of Cbl-b and TRAF6 in quadriceps muscle between DR and cisplatin (Figs. 3C and D). It has been reported that the transcriptional regulation of MAFbx and MuRF1 occurs via forkhead box O1 (FOXO1) and FOXO3 (Sandri et al., 2004; Stitt et al., 2004). The mRNA expression levels of FOXO1 and FOXO3 were increased by DR compared to the vehicle control, and the mRNA expression of FOXO3, but not FOXO1, was further increased by the administration of cisplatin (Figs. 3E and F). There was no difference in mRNA expression levels of MAFbx, MuRF1, Cbl-b, TRAF6, FOXO1 and FOXO3 in quadriceps muscle between vehicle control and cisplatin (1 mg/kg) groups (Figs. 3A-F).

Table 1
Primers for current study.

	Accession no.	Primers		Product size
GAPDH	NM_008084.2	Forward	CCTCGTCCCGTAGACAAAATG	100
		Reverse	TCTCCACTTTGCCACTGCAA	
MAFbx	NM_026346.3	Forward	AGAAAAGCGGCAGCTTCGT	100
		Reverse	GCTGCGACGTCGTAGTTCAG	
MuRT1	NM_001039048.2	Forward	ACACAACCTCTGCCGGAAGT	103
		Reverse	ACGGAAACGACCTCCAGACA	
Cbl-b	NM_001033238.1	Forward	GGACTAACCAGGTGATGGGATGT	99
		Reverse	CCATTCTACTGTGCCTCCCATT	
TRAF6	NM_009424.2	Forward	GCGTGTACGATCGGGTTGT	102
		Reverse	CCAACTATCCCTTCAGCTCCAA	
FOXO1	NM_019739.3	Forward	TCATCACCAAGGCCATCGA	105
		Reverse	TGTCGCCCTTATCCTTGAAGTAG	
FOXO3	NM_019740.2	Forward	TGTTTGGACCTTCGTCTCTGAAC	107
		Reverse	TGTCTGGTTGCCGTAGTGTGA	
IGF-1	NM_010512.4	Forward	GACAGGCATTGTGGATGAGTGT	100
		Reverse	GATAGAGCGGGCTGCTTTTG	
Mstn	NM_010834.2	Forward	AGTAAGCTGCGCCTGGAAAC	109
		Reverse	TCTGGACGTCGTACTGATCGAT	
p21	NM_007669.4	Forward	TACAAGGAGCCAGGCCAAGA	105
		Reverse	GCTTTGACACCCACGGTATTC	
TNF-alpha	NM_013693.2	Forward	GGCAGGTTCTGTCCCTTTCA	115
		Reverse	GGAGTGCCTCTTCTGCCAGTT	
IL-6	NM_031168.1	Forward	GACTTCCATCCAGTTGCCTTCT	115
		Reverse	AGACAGGTCTGTTGGGAGTGGTA	
IL-1beta	NM_008361.3	Forward	TCGTGCTGTCGGACCCATAT	111
		Reverse	TGTCGTTGCTTGGTTCTCCTT	
Cox2	NM_011198.3	Forward	TGAGTACCGCAAACGCTTCTC	105
		Reverse	TCGATGTCACTGTAGAGGGCTTT	

Effects of DR and cisplatin on the gene expression of proinflammatory cytokines and Cox2 in the muscle

We also examined the effects of DR and cisplatin on the gene expression of proinflammatory cytokines and Cox2 in the quadriceps muscle. There were no changes in mRNA expression levels of proinflammatory cytokines (TNF-α, IL-6 and IL-1b) and Cox2 in quadriceps muscle among all groups (Fig. 4).

Effects of DR and cisplatin on the gene expression of IGF-1 and Mstn in the muscle

We next examined the tissue distribution of IGF-1 and Mstn gene expression. The IGF-1 gene was found in various tissues (tongue, bronchus, trachea, liver, aorta, vas deferens, quadriceps muscle, pancreas, testis and so on) and IGF-1 was expressed mostly in the liver (Fig. 5A). The gene expression of IGF-1 in the liver was not changed by DR or cisplatin (3 mg/kg), compared to the vehicle control (Fig. 5B). On the other hand, IGF mRNA in the quadriceps muscle was decreased by DR and cisplatin (3 mg/kg) to the same degree, compared to vehicle (Fig. 5C).

The mRNA expression of Mstn was found in the tongue, esophagus, skin and quadriceps muscle. Among the tissues used in this study, the mRNA level of Mstn was highest in the quadriceps muscle (Fig. 6A). The mRNA of Mstn in the quadriceps muscle was significantly increased by the administration of cisplatin, compared to the vehicle control and DR groups (Fig. 6B). It has been documented that Mstn suppresses muscle cell growth via transcriptional upregulation of the cyclin-dependent kinase (Cdk) inhibitor p21 (Thomas et al., 2000). Therefore, we further investigated whether the administration of cisplatin could influence the expression profiles of p21 in skeletal muscle. The mRNA expression of p21 was significantly increased by the administration of cisplatin compared to that in the vehicle and DR groups (Fig. 6C).

Effects of DR and cisplatin on the expression and phosphorylation of Akt, FOXO3a and Smad-2 in the muscle

Finally, we performed immunoblotting to investigate the protein expression of MuRF1 and MAFbx, and the phosphorylation levels of Akt, FOXO3 and the intracellular effector Mad homolog 2 (Smad2) in the quadriceps muscle among the vehicle control, DR and cisplatin (3 mg/kg) groups. The expression of MuRF1 and MAFbx proteins correlated with their mRNA expression, and was increased in the DR group compared to the vehicle control. Furthermore, their expressions were significantly increased by cisplatin (3 mg/kg) treatment compared to DR (Figs. 7A–C). Phosphorylated Akt was slightly decreased by DR compared to the vehicle control. Akt phosphorylation was significantly decreased by the administration of cisplatin, compared to DR, while there was no difference in the expression level of Akt among the vehicle control, DR and cisplatin groups (Figs. 7A, D and E). FOXO3a expression was increased by the administration of cisplatin, while the phosphorylation of FOXO3a was at a lower level than that in the DR group (Figs. 7F and G). Phosphorylated Smad2 was increased by DR compared to the vehicle control. The phosphorylation of Smad2 was further increased by the administration of cisplatin compared to DR, while there was no difference in the expression level of Smad among these groups (Figs. 7A, H and I).

Discussion

Little information is available regarding anti-cancer drug-induced muscle atrophy. Therefore, in the present study we examined whether the administration of cisplatin could cause muscle atrophy.

MAFbx and MuRF1 were first identified following transcript profiling in fasting and immobilization models of rodent muscle atrophy (Bodine et al., 2001; Gomes et al., 2001). Consistent increases in their gene expression have been observed in a wide range of in vivo models of skeletal muscle atrophy, including diabetes, cancer, renal failure, denervation, unweighting and glucocorticoid or cytokine treatment (Foletta et al., 2011). In the present study, we applied dietary restriction (DR) as a control, rather than fasting, in mice. DR increased the mRNA levels of MAFbx and MuRF1. Interestingly, the levels of MAFbx and MuRF1 were further increased by the administration of cisplatin, although body weight and food intake were at the same levels in these groups. Previous studies have shown that transcriptional regulation, either by direct or indirect means, of MAFbx and MuRF1 in mice occurs via the family of FOXO transcription factors (Sandri et al., 2004; Stitt et al., 2004). FOXO1 does not directly increase the levels of MAFbx or MuRF1, but instead blocks the insulin-like growth factor I (IGF-1)-induced inhibition of their upregulation (Stitt et al., 2004). FOXO3a binds directly to the MAFbx promoter in mouse muscle to increase its transcription (Sandri et al., 2004). Furthermore, Suzuki et al. (2007) demonstrated that FOXO3a upregulates the expression of MuRF1 and MAFbx. In the present study, we found that the expression levels of FOXO1 and FOXO3 were upregulated by DR, while only the FOXO3 level was further increased by the administration of cisplatin (3 mg/kg) compared to the DR group. These results suggest that the increased levels of MAFbx and MuRF1 that occur via the upregulation of FOXO3 by cisplatin may play an important role in cisplatin-induced muscle atrophy.

Many cell types, including skeletal muscle, respond to IGF-I. IGF-I promotes growth by binding to and activating IGF-IR. Activation of the phosphoinositide 3-kinase (PI3K)/Akt signaling pathway by IGF-1/IGF-1R can induce skeletal muscle hypertrophy. Akt is a serine–threonine protein kinase that can induce protein synthesis and block the transcriptional upregulation of key mediators of skeletal muscle atrophy, MuRF1 and MAFbx, by phosphorylating and thereby inhibiting the nuclear translocation of the FOXO family of transcription factors. Once phosphorylated by Akt, FOXOs are excluded from the nucleus, and the upregulation of MuRF1 and MAFbx is blocked (Glass, 2010). In the present study, the phosphorylation of Akt and FOXO3 was dramatically

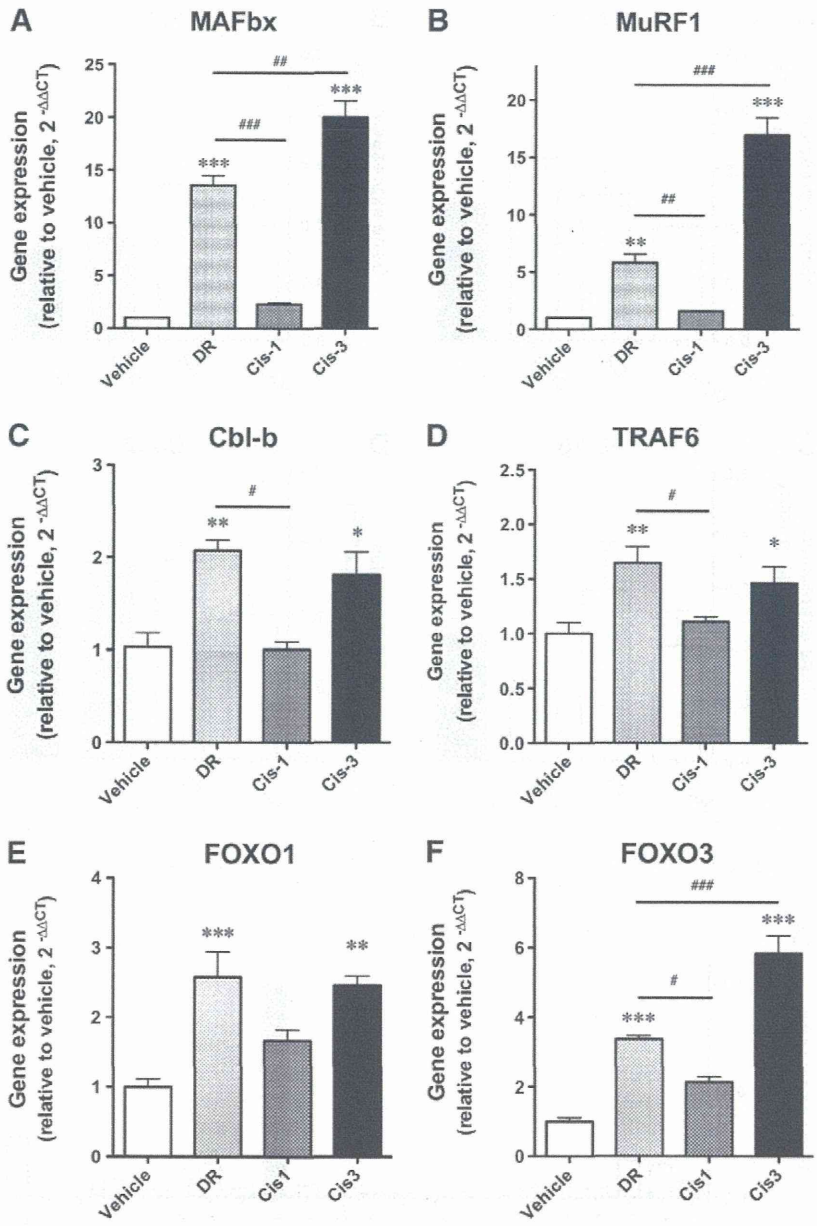

Fig. 3. Effects of DR and cisplatin on the gene expression of MAFbx (A), MuRF1 (B), Cbl-b (C), TRAF6 (D), FOXO1 (E) and FOXO3 (F) in the quadriceps muscle of mice. Each value represents the mean ± S.E.M. from 4 to 8 independent mice. *$p < 0.05$, **$p < 0.01$ and ***$p < 0.001$ vs. vehicle control (saline). ##$p < 0.01$ and ###$p < 0.001$ vs. DR.

reduced by the administration of cisplatin (3 mg/kg), compared to those in the DR group. These findings suggest that the unphosphorylation of Akt may augment the expression of MuRF1 and MAFbx through the unphosphorylation of FOXO3.

Myostatin (Mstn), a member of the TGF-β family, is expressed and secreted predominantly by skeletal muscle, and functions as a negative regulator of muscle growth (McPherron et al., 1997). Mstn binds to ActRIIB, the high-affinity type-2 activin receptor, on muscle membranes (Lee, 2008). This, in turn, activates the type-1 receptor activin receptor-like kinase 4 (ALK4) or ALK5 at the plasma membrane (Rebbapragada et al., 2003; Rios et al., 2004). The activation of a heteromeric receptor complex consisting of type II and type I serine/threonine kinase receptors induces the phosphorylation of intracellular effectors Mad homolog 2 (Smad2) and Smad3 (Rebbapragada et al., 2003; Rios et al., 2004). Phosphorylated Smad2 and Smad3 translocate from the cytoplasm to the nucleus, where they regulate the transcription of specific target genes. It has been reported that Mstn protein and the Mstn/ActRIIB signaling pathway are upregulated in disease states involving cancer to cause muscle wasting (Costelli et al., 2008; Reardon et al., 2001; Seder et al., 2009; Wildi et al., 2001; Yarasheski et al., 2002). Zhou et al. (2010) has been demonstrated that in cancer cachexia models, ActRIIB pathway blockade abolished the activation of the ubiquitin–proteasome system and the induction of muscle-specific E3 ubiquitin ligases in muscles. In the present study, the level of Mstn mRNA in the quadriceps muscle was upregulated by cisplatin, compared to that in the DR group. We found that cisplatin increased the phosphorylation of Smad2 compared to DR, thus confirming activation downstream of the Mstn/ActRIIB signaling pathway.

The present study showed that loss of body weight was similar in DR and cisplatin treated groups, while muscle mass was less and the expression of MuRF1 and MAFbx was higher in cisplatin treated animals. The gene expression of Mstn was significantly increased in cisplatin treated group compared with DR, although the gene expression of Mstn is not significantly different between vehicle control and